Lawrence Berkeley National Laboratory
Recent Work

Title
Ni, Pd AND Pt ON GaAs: A COMPARATIVE STUDY OF REACTED FILM MORPHOLOGIES

Permalink
https://escholarship.org/uc/item/0qj113kb

Author
Sands, T.

Publication Date
1986-04-01

eScholarship.org Powered by the California Digital Library
University of California

LBL-21060
Preprint c.2

Lawrence Berkeley Laboratory

UNIVERSITY OF CALIFORNIA

Materials & Molecular Research Division

RECEIVED
LAWRENCE
BERKELEY LABORATORY

JUN 18 1986

LIBRARY AND
DOCUMENTS SECTION

Submitted to Journal of Materials Research

Ni, Pd AND Pt ON GaAs: A COMPARATIVE STUDY OF REACTED FILM MORPHOLOGIES

T. Sands, V.G. Keramidas, A.J. Yu, K.M. Yu, R. Gronsky and J. Washburn

April 1986

TWO-WEEK LOAN COPY

This is a Library Circulating Copy which may be borrowed for two weeks.

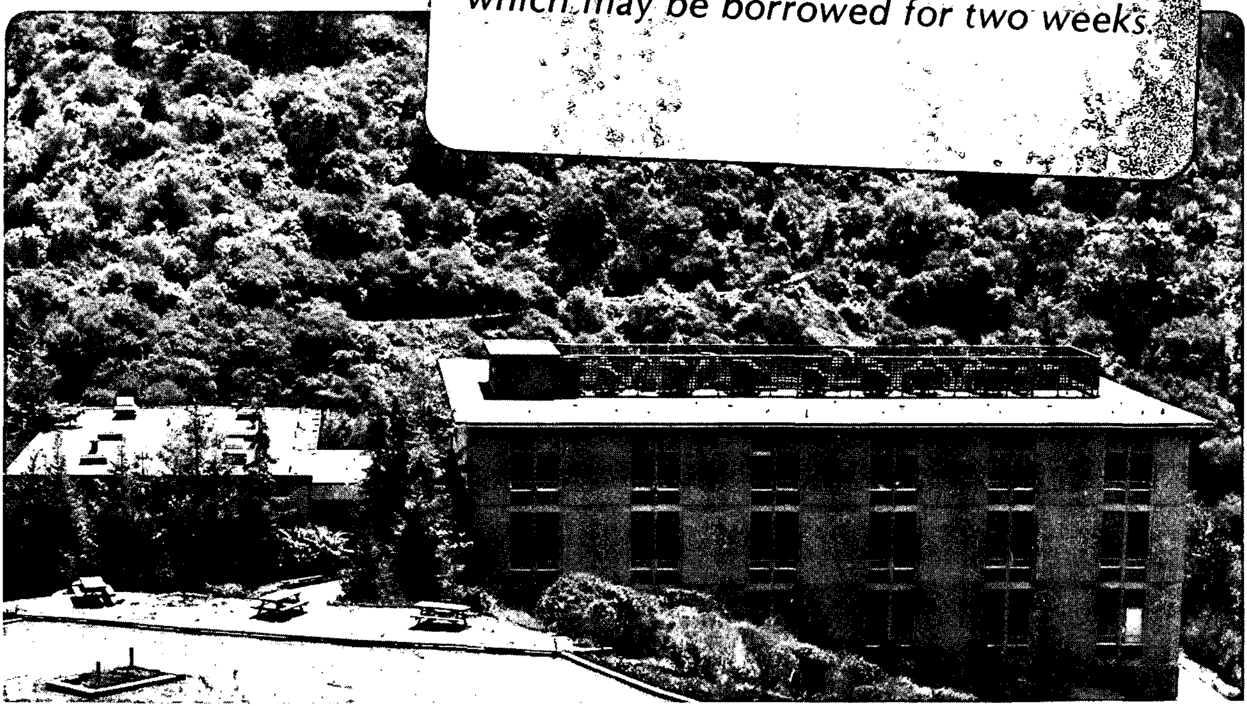

LBL-21060 c.2

Prepared for the U.S. Department of Energy under Contract DE-AC03-76SF00098

DISCLAIMER

This document was prepared as an account of work sponsored by the United States Government. While this document is believed to contain correct information, neither the United States Government nor any agency thereof, nor the Regents of the University of California, nor any of their employees, makes any warranty, express or implied, or assumes any legal responsibility for the accuracy, completeness, or usefulness of any information, apparatus, product, or process disclosed, or represents that its use would not infringe privately owned rights. Reference herein to any specific commercial product, process, or service by its trade name, trademark, manufacturer, or otherwise, does not necessarily constitute or imply its endorsement, recommendation, or favoring by the United States Government or any agency thereof, or the Regents of the University of California. The views and opinions of authors expressed herein do not necessarily state or reflect those of the United States Government or any agency thereof or the Regents of the University of California.

Ni, Pd and Pt on GaAs: A COMPARATIVE STUDY OF REACTED FILM MORPHOLOGIES

T. Sands[a] and V.G. Keramidas
Bell Communications Research, Inc.,
Murray Hill, NJ 07974

A.J. Yu
Department of Materials Science and Engineering,
Cornell University, Ithaca, NY 14583

K.M. Yu, R. Gronsky and J. Washburn
Lawrence Berkeley Laboratory,
University of California,
Berkeley, CA 94720

[a]Work performed as a visiting Industry Fellow at the Center for Advanced Materials, Lawrence Berkeley Laboratory, Berkeley, CA 94720

Ni, Pd and Pt on GaAs: A Comparative Study of Reacted Film Morphologies

T. Sands[a] and V.G. Keramidas
Bell Communications Research, Inc., Murray Hill, NJ 07974

A.J. Yu
Department of Materials Science and Engineering, Cornell University, Ithaca, NY 14583

K.M. Yu, R. Gronsky and J. Washburn
Lawrence Berkeley Laboratory, Berkeley, CA 94720

ABSTRACT

The reactions between (100) GaAs and the near-noble metals Ni, Pd and Pt have been investigated by application of high-resolution transmission electron microscopy (TEM), energy-dispersive analysis of x-rays in the scanning TEM and Rutherford backscattering spectrometry. Emphasis is placed on the evolution of the phase distributions and interface morphologies during annealing at temperatures up to 480°C. The first phase in the Ni/GaAs reaction is shown to have the nominal composition Ni_3GaAs. Ternary phases of the type Pd_xGaAs are also found to be the dominant products of the Pd/GaAs reaction. These observations are used to construct isothermal sections of the M-Ga-As thin-film phase diagrams. The behavior of a thin (1-2nm) native oxide-hydrocarbon layer during the Ni/GaAs, Pd/GaAs and Pt/GaAs reactions is also investigated. Only the Ni/GaAs reaction is noticeably impeded by this

[a] Work performed as a visiting Industry Fellow at the Center for Advanced Materials, Lawrence Berkeley Laboratory, Berkeley, CA 94720

intervening layer. In contrast, the Pd/GaAs and Pt/GaAs reactions tend to mechanically disperse the native oxide layers.

I. INTRODUCTION

Rectifying and low-resistance contacts are essential elements of compound semiconductor electronic and optoelectronic devices. A critical feature of any such contact is the interfacial region between the suitably doped or alloyed compound semiconductor and the first metal or metallic compound layer. This metallurgical interface plays an important role in determining the electrical properties of a rectifying contact. In particular, the structure and chemistry of the interfacial region determine (in ways which are not fully understood[1-7]) the barrier height for electrons or holes. The influence of the metallurgical interface on the electrical properties of a low-resistance contact is even more complex. Braslau,[8] for example has argued that alloyed Au-Ge-based contacts to n-GaAs derive their ohmic properties from an inhomogeneous distribution of microscopic low-resistance current paths. Consequently, spreading resistance in the substrate dominates the measured specific contact resistance. As will be discussed below, such low-resistance paths may result from electron tunneling through highly doped n^+-GaAs. In addition, three-dimensional field emission from small-radius protrusions can significantly reduce the measured barrier height.[9] The latter effect has been invoked by Leung _et al_[10] to explain their experimental data on Au-Ga/GaAs.

It is clear from the above examples that efforts to design new contact metallization schemes would benefit greatly from an enhanced understanding of the structure, chemistry and morphology of contact/compound semiconductor interfaces. Such information becomes essential with the ongoing miniaturization and integration of compound semiconductor devices. As device dimensions become smaller, contacts must be laterally uniform on a scale which is small relative to the contact dimensions. If the average spacing between low-resistance current paths were comparable to or greater than the relevant contact dimensions, then the specific resistance of Au-Ge-based ohmic contacts, for instance, would be highly variable. In addition to lateral nonuniformity, precise control of the penetration depth of the metallization is necessary for contacting shallow layers or buried heterojunctions, both very common in today's devices. Such morphological constraints along with considerations of adherence and stability have motivated recent investigations of ohmic contacts formed by solid-phase reactions as a substitute for eutectic or "alloyed" contacts[11-14]. Nearly every reported GaAs ohmic contact scheme employing solid-phase reactions involves one of the "near-noble" metals, Ni, Pd or Pt[12-14]. The near-noble metals are particularly suitable for this application because of i) ease of deposition, ii) low reaction temperatures with GaAs, iii) compound formation with both Ga and As and iv) resistance to oxidation (especially Pd and Pt).

Despite the interest in these systems, little is known regarding phase formation and the morphological evolution of near-noble metal/GaAs couples. In this paper, we present a comparative study of the Ni/GaAs, Pd/GaAs and Pt/GaAs reactions preceded by a brief review of the role of near-noble metals in current ohmic contact metallization schemes. Emphasis is placed on the determination of the structure, composition and spatial distribution of reaction products with particular attention to ternary phases of the type M_xGaAs (M = Ni or Pd). Since the results of the Pd/GaAs study have been published in detail,[15] they will be discussed only briefly here for comparative purposes.

II. ROLE OF NEAR-NOBLE METALS IN THE FORMATION OF OHMIC CONTACTS TO n-GaAs

A. Ni/GaAs

Layers of pure Au or Au-Ge eutectic alloys on n-GaAs tend to "ball-up" during annealing. This problem is alleviated by the addition of Ni,[14] resulting in enhanced wetting of the contact layer and improved uniformity.[17] The precise role of Ni in determining the specific contact resistance, however, is not yet clear. The electron microscopy data of Kuan *et al*[18] reveal a correlation between specific resistance and the interfacial phase distribution. The contacts with the lowest specific resistances contained a large areal fraction of Ni_2GeAs grains at the interface with GaAs, whereas contacts containing larger areal fractions of Au(Ga)/GaAs interfaces

exhibited higher specific contact resistances .[18] Braslau has suggested that local melting of the eutectic alloy and subsequent regrowth of n^+ Ge-doped GaAs results in an inhomogeneous distribution of low-resistance current paths.[8] The low resistance of these regrown regions is probably due to the tunneling of electrons through the n^+-GaAs. Kuan et al's[18] results provide experimental support for the Braslau model, suggesting that the low resistance current paths are Ni_2GeAs/GaAs interfaces. In Kuan et al's more specific model, Ni reacts to form NiAs which acts as a transport medium for Ge such that the final state is Ni_2GeAs on Ge-doped GaAs. A similar model for the role of Ni in Ni/Ge/GaAs contacts was proposed earlier by Anderson et al.[11]

Recent experiments with simpler systems suggest a second possible role for Ni. Since Au reacts strongly with electropositive Ga but forms no compounds with As, one would expect the Au/GaAs reaction to result in the accummulation of point defects related to excess As (e.g. As_{Ga} antisite defects or As clusters) in the GaAs adjacent to the interface. Such As accumulation has been detected by Liliental et al[19] using x-ray microanalysis in a scanning transmission electron microscope (STEM). These point defects or anion clusters may be responsible for pinning the Fermi level near midgap.[2,6] In an effort to circumvent this problem, Williams et al[20] have deposited the equilibrium phase $AuGa_2$ onto GaAs by molecular beam epitaxy. The resulting contact exhibited ohmic

behavior. It is therefore plausible that Ni and Ge act as sinks for the excess As produced by the Au/GaAs reaction. One would then expect the Au(Ga)/GaAs interfaces adjacent to grains of Ni_2GeAs to be free from interfacial accumulations of As, thus permitting ohmic conduction.

Taking a different approach, Smith and Solomon[13] have eliminated the Au as an active component. Their preliminary electrical results suggest that an ohmic contact can be formed by ion-beam mixing of Ni/GaAs with Ge^+. Similarly, Anderson et al[11] produced an ohmic contact by sintering Ni/Ge/GaAs. The presence of Ni enhanced the indiffusion of Ge, perhaps creating a n+ GaAs layer at the Ni-Ge/GaAs interface.[11] These procedures have the advantage of involving only solid-phase reactions. A sufficiently low specific resistance ($<10^{-6}$ Ω -cm^2), however, has not yet been demonstrated.

In an attempt to simplify the system and elucidate the role of Ni, Ogawa[21] studied the Ni/GaAs reaction. Nickel was shown to react with GaAs at low temperatures ($\gtrsim$ 200° C) to form a ternary Ni_xGaAs phase. Quantitation of Auger electron spectroscopy (AES) data yielded the composition Ni_2GaAs. Above 400° C, Ogawa observed the binary phases Ni-Ga and NiAs suggesting that Ni_2GaAs might be a metastable phase. Lahav et al[22] made similar observations using transmission electron microscopy (TEM) and AES. The energy dispersive x-ray data of Sands et al[23], however, are consistent with a nominal composition of Ni_3GaAs for the ternary phase. In

the following sections, further evidence for this latter result is presented. The evolution of the reacted film morphology at higher temperatures (>400° C) is also discussed.

B. Pd/GaAs

In a variation on earlier experiments with Pd-Ge/n-GaAs,[24] Marshall *et al*[12] have fabricated a non-alloyed contact to n-GaAs which employs Pd as a metallic transport medium for Ge. During annealing at 325°C, Ge diffuses through the reacted Pd layer and grows epitaxially on the GaAs. It is interesting that, contrary to expectations, an ohmic contact is formed even if the Ge is not intentionally doped.[24] Thus, Pd may play a role larger than that of a transport medium.

The precise metallurgical behavior of Pd in multilayered structures has not yet been established. In fact, the metallurgical behavior of Pd in even the simpler Pd/GaAs system has only recently been clarified. Early x-ray diffraction studies of the Pd/GaAs reaction suggested the formation of $PdAs_2$, PdGa and Pd_2Ga as the major reaction products.[25-26] Subsequent TEM studies however, showed that the first phase, designated in this paper as "phase I" for clarity, is a ternary phase, Pd_xGaAs,[15,27-29] and has a hexagonal unit cell with lattice parameters a_o = 0.67 nm and c_o= 0.34 nm.[28-29]. Combining etching studies with TEM, Sands *et al*[30] have demonstrated the orientation relationship $[0001]_I//[01\bar{1}]_{GaAs}$ and $(\bar{2}110)_I//(100)_{GaAs}$ with (100) GaAs. Grains of phase I with $[0001]_I$ // $[011]_{GaAs}$ are not observed. This orientation

relationship is believed to result from the preferential growth of phase I nuclei which are oriented such that [0001], the fastest growth direction in phase I, is parallel to [01$\bar{1}$], the fastest etching direction in the (100) plane of GaAs.[30]

The composition of phase I is still argued in the literature. Composition estimates range from Pd_2GaAs[31] to $Pd_4Ga_{\sim 1.2}As_{\sim 0.8}$.[27] It has been clearly established, however, that phase I can accommodate deviations from Ga:As = 1 resulting from the sublimation of As.[15,27,30]

A second ternary phase, "phase II", has been detected in films annealed above 250°C. Phase II is the dominant phase in films annealed in the temperature range 300 to ~450°C, depending on the film thickness and annealing environment.[15,27,30] Phase II is also hexagonal with $a_o \cong 0.9$ nm and $c_o \cong 0.37$ nm.[28,29] Composition estimates for phase II range from ~ Pd_4GaAs for 19-60 nm Pd annealed at temperatures between 275 and 480°C[30] to $Pd_2Ga_{\sim 1.2}As_{\sim 0.8}$ for 15 nm Pd annealed at 350°C in forming gas.[27] Like phase I, phase II can accommodate substantial variation in Ga:As; up to ~ 2 in a sample annealed at 480°C[15]

The discrepancies between the x-ray studies[25,26] which identified PdGa, $PdAs_2$ and Pd_2Ga at low temperatures ($\lesssim$350°C), and the TEM investigations[15,27-30] which report two ternary phases have been discussed by Sands *et al*.[15] Since the ternary phase peaks overlap with the binary phase peaks in

glancing-angle x-ray diffraction spectra, it is very likely that phases I and II have been misidentified as PdGa and $PdAs_2$, respectively.

C. Pt/GaAs

Platinum has been used as a gate electrode to n-GaAs in recent integrated circuit designs.[32] Formation of ohmic contacts by Si^+ ion-mixing of Pt/n-GaAs has also been demonstrated.[14] Unlike Ni, Pt is a heavier element than either Ga or As. Unlike Pd, Pt reacts with GaAs to form laterally uniform layers. Consequently, the Pt/GaAs reaction can be studied by relatively straightforward application of Rutherford backscattering spectrometry (RBS). Combined with x-ray or electron diffraction, RBS studies have shown that complete reaction results in the layer sequence PtGa/$PtAs_2$/GaAs.[33,34] The initial stages of the reaction involve the diffusion of Ga into the Pt layer, consistent with the large difference in the electronegativities of these elements. Simultaneously, Pt begins to react with As to form an interfacial layer of $PtAs_2$. Fontaine *et al*[35] have shown that this $PtAs_2$ layer is highly textured. In the following sections the development of this PtGa/$PtAs_2$/GaAs layer sequence is compared with the evolution of the Ni_xGaAs and Pd_xGaAs reacted layers by application of cross-sectional TEM and RBS.

III. EXPERIMENTAL METHODS

Undoped semi-insulating (100) LEC GaAs substrates were prepared for metal deposition by immersion into a 9:1 deionized

H_2O:HCl solution for 10 sec. followed by a rinse in deionized H_2O. Samples were then blown dry with N_2 and inserted into the deposition chamber. Films of either Ni, Pd or Pt were deposited by electron beam evaporation to a thickness of $\sim$45nm in a vacuum of 1-2 x 10^{-6} torr.

Both plan-view and cross-sectional specimens were prepared by standard techniques described in Reference 36. It should be noted that plan-view and cross-sectional specimens experienced a maximum temperature of $\sim$80°C for up to 5 min. during the specimen preparation process. As a result, the term "as-deposited" in subsequent sections implies that the TEM specimen has experienced a mild thermal treatment.

Samples were annealed at 220, 275, 315, 410 and 480°C for 10 min. in flowing forming gas (95% Ar, 5% H_2). For each annealing treatment, samples of Ni/GaAs, Pd/GaAs and Pt/GaAs were annealed simultaneously to ensure the validity of direct comparisons.

Plan-view specimens were examined in a Siemens 102 TEM at 100 keV. Images and selected-area diffraction patterns provided a rapid assessment of phase identity and lateral film uniformity. Cross-sectional TEM specimens from each sample were imaged at 200 kV in a JEOL JEM 200CX equipped with a high-resolution ($\sim$0.25nm point-to-point) pole piece. High-resolution and two-beam images in the $[011]_{GaAs}$, $[01\bar{1}]_{GaAs}$ and $\langle 001\rangle_{GaAs}$ zone-axis directions provided a detailed description of the distribution of phases in depth. When

chemical information was required, both plan-view and cross-sectional samples were analyzed in a JEOL JEM 200CX analytical TEM/STEM equipped with Kevex high-angle and ultra-thin-window x-ray detectors. Energy dispersive x-ray spectra (EDS) were analyzed using spectra from the GaAs substrates as standards. In the absence of reliable M-Ga and M-As standards (M=Ni,Pd or Pt), theoretical k-factors[37] were applied. Where possible, these interpretations of the EDS data have been checked by comparison with composition estimates using alternative techniques such as RBS and the measurement of layer thicknesses.

IV. RESULTS AND DISCUSSION

A. Ni/GaAs

Nickel reacts readily with GaAs during deposition (and/or during TEM specimen preparation). A reacted layer 3-5 nm thick can be seen in Fig. 1 below the thin (1-2nm) native oxide-hydrocarbon layer. By calibrating the image magnification using lattice images of the adjacent GaAs substrate, accurate measurements of layer thicknesses can be made. Using this technique it was found that 44 ± 2 nm of Ni annealed at 220°C for 10 min. reacted with GaAs to form 88 ± 2 nm of a Ni-Ga-As phase (or phases). The reaction is highly uniform except where inhibited by disk-shaped patches of the native oxide-hydrocarbon layer. These unreacted regions account for $\sim$10 percent of the sample surface area and appear as holes or thin areas in plan-view TEM specimens since the etchant

"lifts off" the unreacted Ni by dissolving the intervening oxide (see Fig. 2). In the cross-section micrograph shown in Fig. 3 the morphology of these patches is clearly revealed. Note that the native oxide-hydrocarbon layer, which remains smooth and intact throughout the reaction, ends up on the surface of the reacted layer when the reaction is complete. Similar behavior was not observed for the Pd/GaAs and Pt/GaAs reactions, even though the identical cleaning procedure was used. As will be shown in following sections, these latter reactions involve the mechanical dispersion of the native oxide-hydrocarbon layer.

Although the morphology in Fig. 3 is not desirable from the device standpoint, such images clearly show that Ni is the dominant moving species. Furthermore, images such as Fig. 3 provide an opportunity to measure the amount of GaAs consumed by the Ni/GaAs reaction. The atomic concentration in Ni and GaAs ($[Ni]_{Ni} = 9.14 \times 10^{22}$ atoms/cm^3 and $[Ga]_{GaAs} = [As]_{GaAs} = 2.22 \times 10^{22}$ atoms/cm^3) combined with the layer thickness measurements shown in Fig. 4 yield an average composition of $Ni_{3.0\pm0.2}GaAs$ for the reacted layer. This nominal composition is confirmed by the EDS results in Fig. 5(a) and (b). Standardless quantitation of these spectra using theoretical k factors[37] gives a value of x in Ni_xGaAs of 2.9 with a standard deviation of 0.24. The EDS results also suggest that sublimation of As from the reacted layer is significant, even at temperatures as low as 315°C. Using the GaAs

substrate as a standard yields Ga:As ratios of 1.07 and 1.28 for the samples annealed at 220 and 315° C, respectively.

In an effort to verify the compositional measurements reported above, the sample annealed at 220° C was analyzed by RBS. Using the TEM data as input to a simulation program developed at Cornell University,[38] the RBS data in Fig. 6 is shown to be consistent with the EDS and layer thickness measurements. Thus, the nominal composition of the reacted layer at low temperatures measured by these three largely independent techniques using the same samples is $\sim Ni_3GaAs$.

Electron diffraction was used to assess the structure of the Ni_3GaAs films. As reported previously,[22,39] the film was found to consist of four twin-related variants of a hexagonal unit cell with lattice parameters $a_o \cong 0.4$nm and $c_o \cong 0.5$ nm. The orientation relationship with (100) was determined to be

$$\{0\bar{1}1\}_{GaAs} \mathbin{//} \{01\bar{1}2\}_{Ni_xGaAs}$$

and

$$\langle 011\rangle_{GaAs} \mathbin{//} \langle 2\bar{1}\bar{1}0\rangle_{Ni_xGaAs}$$

Figure 7 shows diffraction patterns from cross-sectional and plan-view specimens that illustrate the above orientation relationship. Unlike previous investigations,[21,22,39] we found that $\{0001\}_{Ni_xGaAs}$ was not precisely oriented parallel to $\{111\}_{GaAs}$. The misorientation between these planes was found to depend on the c_o/a_o ratio as would be expected for the orientation relationship reported here. As noted by Lahav

et al,[22] a c_o/a_o ratio of $\sqrt{3}/\sqrt{2} = 1.2248$ would satisfy the above orientation relationship in addition to the condition $\{0001\}_{Ni_xGaAs}$ // $\{111\}_{GaAs}$. Such a "pseudocubic" c_o/a_o ratio would also dictate that the spacings of the $\{01\bar{1}2\}$ and $\{2\bar{1}\bar{1}0\}$ planes would be equal. As shown in Table I, $d\{01\bar{1}2\}$ / $d\{2\bar{1}\bar{1}0\}$ varies from 1.032 to 1.079 with annealing temperature in our samples. Since the $\{01\bar{1}2\}$ and $\{2\bar{1}\bar{1}0\}$ planes of overlapping variants are parallel, this deviation from $c_o/a_o = \sqrt{3}/\sqrt{2}$ is directly visible as vertical moiré fringe contrast in the $\langle 011\rangle_{GaAs}$ cross-sectional images in Fig. 1. Note that the moiré fringe spacing decreases with increasing annealing temperature in accordance with the increase in $d\{01\bar{1}2\}$ / $d\{2\bar{1}\bar{1}0\}$ as indicated in Table I.

The diffraction patterns from Ni_xGaAs films annealed at temperatures up to and including 410°C suggest that the films contain only the single hexagonal phase. Furthermore, EDS spectra obtained with probes as small as 10 nm in diameter showed similar amounts of Ga and As, in agreement with spectra obtained with larger probes. Since the grain size is on the order of 10 nm (see Fig. 2), the EDS spectra should be sufficient to distinguish an intimate mixture of binary Ni-Ga and Ni-As phases from a morphology consisting of a single ternary phase. We therefore conclude that the Ni-Ga-As films consist of a true ternary phase, in agreement with previous studies.[21,22]

In Table I we compare the EDS and diffraction data from Ni_xGaAs with crystallographic data from two binary phases, $Ni_{3.55}Ga_{2.00}$ and NiAs, which adopt the B8 structure. The observation that the lattice parameters of Ni_xGaAs are intermediate between those of $Ni_{3.55}Ga_{2.00}$ and NiAs suggests that Ni_xGaAs may also have the B8 structure. Furthermore, the unit cell volume of Ni_3GaAs as measured by electron diffraction ($\sim$0.066 nm^3) along with the measurements in Fig. 4 yield a unit cell content of one As, one Ga and three Ni atoms. The B8 structure is very accommodating in that the unit cell parameters change only slightly with large changes in cell content. The unit cell of the prototypical B8 phase, NiAs, is depicted in Fig. 8. In this structure the two positions at (1/3,2/3,3/4) and (2/3,1/3,1/4) are unoccupied. The unit cell of a similar phase, Ni_2In, is also depicted in Fig. 8. In this latter material, both positions are occupied by Ni. Thus, Ni_2In adopts a "filled" NiAs-type ($B8_2$) structure.[40] Compositionally, Ni_3GaAs is most similar to γ' Ni_3Ga_2, a low temperature superstructure of γ Ni_xGa.[41] In this "half-filled" B8 unit cell there is only one empty Ni site. The Ni vacancies probably account for the rapid diffusion of Ni through the reacted film. Ordering of these Ni vacancies may give rise to the $2a_o \times c_o$ and $3a_o \times c_o$ superstructures observed in Ni_3GaAs (Fig. 7(b)). Superstructures may also result from ordering of Ga and As on the (1/3, 2/3, 1/4) and (2/3, 1/3, 3/4) sites. Such ordering, however, would lead to very weak superlattice reflections since the difference

in the electron scattering factors of Ga and As is small.

From Fig. 8 and the previous discussion it is clear that the proposed Ni_xGaAs structure could tolerate variations from $x = 2$ to $x = 4$. A similar variation ($2.5 < x < 4$) has been reported recently by Chen et al in an investigation of Ni polycrystalline GaAs lateral diffusion couples.[42] In fact, the lattice parameter measurements in Table I suggest a slight change in composition in our samples as the annealing temperature increased from 220 to 410°C. In particular, the c_o/a_o ratio increases from 1.285 to 1.322 over this annealing temperature range. If one applies the simple model that x in Ni_xX (X = Ga or As) is linearly related to a_o/c_o, and using the values of c_o/a_o for $Ni_{3.55}Ga_{2.00}$[41] and NiAs[43] (1.25 and 1.39, respectively), one obtains estimates for x which agree with the EDS results within experimental error (see Table I). It is also interesting that the c_o/a_o ratios of Ni_xIn_2 (c_o/a_o = 1.228 for $x = 4$ and 1.233 for $x = 3.62$)[40] also fit well with this model. This suggests that c_o/a_o is relatively insensitive to X in Ni_xX_2 where X is In, Ga or As. Consequently, one can obtain a quick estimate for x in a Ni_xGaAs layer by simply measuring the c_o/a_o ratio by x-ray or electron diffraction. Note that this model predicts that $c_o/a_o = \sqrt{3}/\sqrt{2}$ at $x = 3.87$.

The decrease in x with annealing temperature is also reflected in a slight (∿10%) increase in the reacted layer thickness between the samples annealed at 220 and 410°C (Fig.

1). In addition, after annealing at 410°C, small protrusions of a hexagonal phase are visible at the interface with GaAs (Fig. 1). The lateral uniformity of the reacted film breaks down further during annealing at 480°C for 10 min (Fig. 9). In Figure 9 the white line indicates the depth of the reacted layer after annealing at 220°C for 10 min. It is clear that annealing at 480°C has resulted in further consumption of the GaAs substrate. The grain size has also increased to ∿50 nm. Energy dispersive x-ray spectra (e.g. Fig. 5(d)) from grains with the B8 structure as imaged in Fig. 10 (the same grain is arrowed in Fig. 9) show that these interfacial grains have a composition of ∿ $Ni_2Ga_{0.7}As_{1.3}$. Grains toward the surface are Ga-rich (Fig. 5(c)) with average composition $Ni_{2.5}Ga_{1.25}As_{0.75}$. This morphology evidently represents the initial stage of the phase separation as observed by Ogawa[21] and Lahav et al[22]. The formation of an As-rich phase adjacent to the GaAs is also consistent with prior observations.[21]

These TEM results indicate that the high temperature (>400°C) separation into binary Ni-Ga and NiAs phases involves the further consumption of GaAs. Consequently, it is possible that Ni_3GaAs is a stable phase in the ternary system. Ni_3GaAs, however, is not stable in the presence of excess GaAs.

The formation of the arsenic rich $Ni_2Ga_{0.7}As_{1.3}$ phase near the interface may be a consequence of the fact that the binary phase Ni_3Ga_2 is richer in Ni than NiAs. Thus, the initial stages of the phase separation, within the constraints

imposed by the B8 structure, would more naturally involve the formation of the Ni-deficient phase at the interface where GaAs is being consumed. Differences in bonding and interface structure between NiAs/GaAs and Ni_3Ga_2/GaAs may also play a role in determining the layer sequence. After annealing at 600°C for 1 hour Lahav *et al*[22] observed that the phase separation was lateral, the two phases being cubic NiGa and hexagonal NiAs. This observation suggests that as the consumption of GaAs continues the Ga content of the Ga-rich phase increases resulting in the nucleation of cubic NiGa. Lateral separation reduces the NiGa/NiAs interface area, thereby reducing the interfacial contribution to the free energy.

These observations are summarized in the proposed isothermal section of the thin film Ni-Ga-As phase diagram shown in Fig. 11(a). It should be noted that the diagrams in Fig. 11 are schematic and include only those binary and ternary phases which have been detected in the reacted thin films. Therefore, additional tie lines are possible. As discussed by Beyers *et al*,[44] these simplified phase diagrams do, however, provide useful guides to phase formation sequences. For example, by tracing the path of the average reacted film composition as more and more Ga and As is incorporated, we see that during the Ni/GaAs reaction we proceed from Ni to Ni + $Ni_3Ga_{2-y}As_y$ to $Ni_3Ga_{2-y}As_y$ + $Ni_2As_{2-z}Ga_z$ to $Ni_3Ga_{2-y}As_y$ + NiGa + $Ni_2As_{2-z}As_z$ to NiGa + $Ni_2As_{2-z}Ga_z$ where the reaction stops.

B. Pd/GaAs

Like Ni, Pd reacts during deposition (Fig. 1). Unlike Ni, however, the native oxide-hydrocarbon layer as prepared in this study does not prevent the reaction locally. Another difference between the behavior of Pd and Ni is revealed in Fig. 12. Note that the phase I layer which forms during deposition (and TEM specimen preparation) is not completely planar. Rather, this layer is broken up into small grains of phase I which are slightly misoriented relative to adjacent grains. The formation of this atomically rough interface acts to mechanically disperse the native oxide. In contrast, the Ni_xGaAs layer is sufficiently uniform so as to cause little disruption in the local planarity of the native oxide-hydrocarbon layer (Fig. 3). After annealing Pd/GaAs at 220°C for 10 min., the native oxide-hydrocarbon layer can no longer be seen by image contrast (Fig. 1), suggesting that the native oxide-hydrocarbon layer has been completely dispersed. Instead, voids are visible in the Pd above the phase I layer. Both the presence of these voids and the position of the native oxide-hydrocarbon layer in the as-deposited sample indicate that Pd is the dominant moving species at low temperatures.

During annealing between 250 and 275°C, a second Pd_xGaAs phase nucleates at large-angle grain boundaries in the phase I film (Fig. 13). As illustrated in Fig. 14, the formation

of deep penetrations of phase II involves the consumption of the remaining unreacted Pd. Since the nucleation sites for phase II (large-angle grain boundaries in the phase I film) are separated by ∿1μm, the formation of phase II penetrations involves extensive lateral transport of Pd.

Phase II forms with a composition which is dictated by the amount of unreacted Pd. For example, Sands et al[45] found that for thin Pd films (∿15 nm) annealed at 350°C for 20 min., phase II has a composition of ∿$Pd_{3.3}Ga_{1.2}As_{0.8}$ (note that Kuan et al[27] estimated the composition of phase II as ∿$Pd_2Ga_{\sim 1.2}As_{\sim 0.8}$ under similar conditions) whereas for thicker Pd films (~60nm), the composition of phase II is ∿ Pd_4GaAs after annealing under similar conditions.[30] In these thicker films, a considerable amount of Pd remains unreacted when phase II nucleates. For the thinner Pd films, most of the deposited Pd (up to ∿ 15 nm) is consumed by the formation of the phase I layer in the initial stages of the reaction. Consequently, more GaAs than Pd is consumed by the reacted layer during the formation of phase II, resulting in a Pd-deficient composition.

Above ∿350°C, no trace of phase I remains. Since the compositional existence ranges of phase I and phase II apparently overlap (composition measurements of both phases I and II range from ∿Pd_2GaAs to Pd_4GaAs with the precise Ga:As ratios varying from 1-2 depending on annealing environment),[15,23,27,28,30,31,45] phase II must be the stable phase above ∿250° C. Phase I is evidently the stable phase

below 250°C and in the presence of the interface with GaAs. Since phase I is highly oriented on GaAs it is possible that phase I is a metastable phase in the bulk Pd-Ga-As system which is stabilized in the form of a thin film by the reduction in excess interfacial free energy due to epitaxy.

Perhaps the most remarkable difference between the Pd/GaAs and Ni/GaAs reactions was observed after annealing under identical conditions at 480°C for 10 min. In Ni/GaAs this annealing treatment resulted in the stratification of the Ga and As distributions in the Ni-Ga-As layer with a considerable amount of As remaining in the reacted layer near the interface with GaAs (see Fig. 5). In contrast, in Pd/GaAs the As:Ga ratio was reduced to ~ 0.2 by the sublimation of As from phase II ($\sim Pd_4Ga_{1.25}As_{0.75}$). The dominant observed phase was a Pd-Ga phase with composition $Pd_{3.3}Ga_{1.8}As_{0.2}$.[30] Although the detailed explanation for this difference in behavior may be quite complex, it is apparent that morphology influences the degree of As loss. Ni and, as will be discussed below, Pt react to form As-rich compounds at the interface with GaAs. The resulting Ga-rich layers near the surface probably act as protective caps preventing excessive As loss. Palladium, on the other hand, when reacted with GaAs, does not cause extensive stratification of Ga and As. Thus, the As-containing compounds are exposed directly to the annealing ambient resulting in rapid As loss.

These observations for $250^\circ C \leq T \leq 480^\circ C$ are summarized in the schematic isothermal section of the Pd-Ga-As thin-film phase diagram shown in Fig. 11(b). The sequence of phase formation in this model depends on the degree of As loss. If little As is lost during the reaction as in the case of samples capped with SiO_2, the endpoint is either a ternary Pd_xGaAs phase at low temperatures or the binary phases PdGa and $PdAs_2$ at higher temperatures (>600°C)[46]. If significant As loss occurs as seen in this experiment, $Pd_{3.3}Ga_{1.8}As_{0.3}$ or PdGa forms.

C. Pt/GaAs

Of the near-noble metals, only Pt shows no evidence of reaction with GaAs during deposition and specimen preparation (see Fig. 1). Even after annealing at 220°C for 10 min. only a slight reaction is indicated by image contrast below the native oxide-hyrocarbon layer. Annealing at ~315°C for 10 min., however, results in an extensive reaction. In Fig. 1, a ~30nm thick reacted layer can be seen below the native oxide-hydrocarbon layer. Plan-view diffraction patterns (not shown) indicate the presence of $PtAs_2$ and Pt. Structural similarities as discussed by Fontaine et al[35] do not allow us to rule out the possbility that $PtGa_2$ and small amounts of Pt_3Ga are present as well. A Rutherford backscattering spectrum from this sample (Fig. 15) also suggests that the reaction is incomplete and that the probable layer sequence is $Pt/Pt_3Ga/PtAs_2/GaAs$.

After annealing at 410 and 480°C for 10 min. the reaction is nearly complete with only PtGa and $PtAs_2$ as detected by diffraction and RBS. In Fig. 1 it is apparent that the grains of $PtAs_2$ in the interfacial layer have coarsened considerably. Assuming that diffusion of Pt occurs primarily along $PtAs_2$ grain boundaries, this coarsening of the $PtAs_2$ layer may explain the "self-limiting" behavior of the reaction as observed by Kumar.[47]

The high-resolution image of the $PtAs_2$/GaAs interface in Fig. 16 illustrates the dominant twin relationship between the grains of cubic $PtAs_2$ and GaAs. This same orientation relationship was detected by Fontaine _et al_[35] by electron diffraction from plan-view specimens. Comparison between the samples annealed at 315 and 410°C suggests that the grains with the orientation relationship $\langle 011\rangle_{PtAs_2}$ // $\langle 011\rangle_{GaAs}$ and $\{1\bar{2}2\}_{PtAs_2}$ // $\{100\}_{GaAs}$ (so that $\{\bar{1}\bar{1}1\}_{PtAs_2}$ // $\{1\bar{1}1\}_{GaAs}$) grow preferentially during annealing. Variations in growth rate with orientation result in considerable roughening of the $PtAs_2$/GaAs interface. In contrast, the initial stages of the Ni/GaAs reaction involve growth of vertical columnar grains. These Ni_3GaAs grains do not exhibit a detectable deviation from the exact orientation relationship reported in Section IVA. The breakdown in the lateral uniformity of the Ni_3GaAs interface results from further reaction with GaAs followed by phase separation. The roughening of the $PtAs_2$/GaAs interface appears to result from competitive growth of grains

with slightly different orientations.

The significant difference in the behavior of the native oxide-hydrocarbon layer during the Pt/GaAs reaction as compared with the Ni/GaAs and Pd/GaAs reactions is that in Pt/GaAs the final position of the native oxide-hydrocarbon layer is within the reacted film rather than on the surface. Using AES, Chang *et al*[48] also detected an oxide layer between the Pt-Ga and Pt-As reacted layers. This morphology is a consequence of the fact that Ga is also a dominant moving species in this reaction. It is interesting to note that, unlike the Ni/GaAs reaction, the Pt/GaAs reaction does not appear to be greatly inhibited by the thin native oxide-hydrocarbon layer. Evidently, the Pt/GaAs reaction mechanically disperses the native oxide-hydrocarbon layer in a manner similar to the action of Pd on GaAs.

The phase formation sequence in the Pt/GaAs reaction can be summarized by referring to the schematic isothermal section of the ternary phase diagram shown in Fig. 11(c). Only tie lines between phases observed in this study are included.

V. CONCLUSION

In this study we have explored the reactions of Ni, Pd and Pt on (100) GaAs with emphasis on the determination of i) the structure, composition and orientation of the first product phase, ii) the dominant moving species, iii) the role of a thin (1-2nm) native oxide-hydrocarbon layer and iv) the

mechanisms of the breakdown of lateral interface uniformity. This data is summarized in Table II. Of particular interest is the identification of the ternary phase, Ni_xGaAs,[21-23] and the two Pd_xGaAs phases.[15,27,28] Formation of these phases by solid-phase reaction should not result in the accumulation of Ga or As in the GaAs near the interface. Thus, studies of the electronic properties of $M_xGaAs/GaAs$ interfaces may advance the understanding of the factors which determine the barrier height. As more detailed TEM studies of M/GaAs reactions are performed it is likely that other M_xGaAs phases will be discovered. In fact, the recent RBS and TEM results of A.J. Yu et al[49,50] suggest that Co reacts with GaAs to form Co_2GaAs. Similar reaction products can be expected in other $M\text{-}A_{III}B_V$ systems.

Further work is needed in understanding the effects of thin native oxide-hydrocarbon layers on $M/A_{III}B_V$ reactions. In this study we found that only the Ni/GaAs reaction was influenced in a significant way be this intervening layer. The observation that the Ni/GaAs reaction is completely prevented locally (see Fig. 3(a)) suggests an additional effect related to the stronger chemical affinity of Ni for oxygen as indicated by the standard heats of formation for oxides (per oxygen atom) which become more negative in the sequence Pt,Pd, As, Ni, Ga. The exact nature of the interaction between Ni and the native oxide of GaAs, however, remains unclear. From a practical standpoint the mechanical dispersion of the

intervening oxide layer by the Pd/GaAs reaction at low temperatures (<100°C) suggests that a thin layer of Pd ($\lesssim$10nm) placed between the substrate and the deposited contact metals may promote a more uniform reaction during the subsequent annealing treatment.

ACKNOWLEDGEMENTS

The authors gratefully acknowledge the assistance provided by the staff of the National Center for Electron Microscopy, Lawrence Berkeley Laboratory. The technical contributions of Grace King, are also greatly appreciated. One of the authors (A.J. Yu) would like to acknowledge the support of the Defense Advanced Research Project Agency under Contract No. N6600-1-83-C-0304 monitored by the Naval Ocean System Center.

This work was supported by the Director, Office of Energy Research, Office of Basic Energy Sciences, Materials Sciences Division of the U.S. Department of Energy under Contract No. DE-AC03-76SF00098.

Table I.

Compositions and Lattice Parameters of Ni-Ga-As Phases with the B8 Structure

Annealing T[C°]	Compositions measured	Compositions calculated[a]	Lattice Parameters a_o[nm]	c_o[nm]	c_o/a_o	$d_{01\bar{1}2}/d_{2\bar{1}\bar{1}0}$
	$Ni_{3.55}Ga_{2.00}$[b]	---	0.400	0.498	1.25	1.011
220[c]	$Ni_{\sim3}Ga_{1.03}As_{0.97}$	$Ni_{3.1}X_2$	0.390±0.001	0.501±0.002	1.285±0.005	1.032±0.004
315[c]	$Ni_{\sim3}Ga_{1.12}As_{0.88}$	$Ni_{2.9}X_2$	0.388±0.001	0.507±0.002	1.305±0.005	1.043±0.004
410[c]	---	$Ni_{2.7}X_2$	0.379±0.001	0.501±0.002	1.322±0.005	1.051±0.004
480[c]	$Ni_{\sim2}Ga_{0.71}As_{1.29}$[d]	$Ni_{2.2}X_2$	0.364±0.001	0.499±0.002	1.371±0.005	1.079±0.004
	NiAs[e]	---	0.362	0.503	1.39	1.084

[a] Calculated assuming a linear relationship between a_o/c_o and x in Ni_xX_2 where X = As or Ga.

[b] See Reference 41.

[c] This study. Compositions measured by EDS.

[d] Composition and lattice parameter measurements from Ni-Ga-As grain at interface. Near-surface grains are Ga rich.

[e] See Reference 43.

Table II

Data Summary: Ni, Pd and Pt (∼45nm) on GaAs

	Reaction initiation temperature [°C]	First reacted phase at M/GaAs interface	Structure and lattice parameters of first phase	Orientation relationship of first phase with GaAs	Other phases formed	Dominant moving species	Position of native oxide after reaction	Temp. and mechanism of break-down in lateraly uniformity	Final phase distribution after annealing in forming gas
Ni	as-deposited	$Ni_xGa_{2-y}As_y$ ($x\simeq 3, y\lesssim 1$)	Ni_3Ga_2-type (B8, hexagonal) $a_o \simeq 0.39$ nm $c_o \simeq 0.50$ nm	$\langle 2\bar{1}\bar{1}0\rangle \| \langle 011\rangle_{GaAs}$ $(01\bar{1}2) \| (0\bar{1}1)_{GaAs}$ very highly textured	$Ni_2As_{2-z}Ga_z$ ($z\leq 0.75$), cubic NiGa	Ni	surface	∼400°C further reaction with GaAs, phase separation	NiGa/GaAs[b] and NiAs/GaAs (∼600°C)
Pd	as-deposited	$Pd_xGa_{1+y}As_{1-y}$ (phase I, $3\leq x\leq 4$, $y\leq 0.3$)	Pd_2Si-type[a] (hexagonal) $a_o \simeq 0.67$ nm $c_o \simeq 0.34$ nm	$[0001] \| [01\bar{1}]_{GaAs}$ $(\bar{2}110) \| (100)_{GaAs}$ highly textured	$Pd_xGa_{1+y}As_{1-y}$ (phase II, $2\leq x\leq 4$, $y\leq 0.3$), Pd-Ga	Pd	surface	∼250°C rapid surface migration of Pd, nucleation of phase II	Pd-Ga/GaAs (∼500°C)
Pt	$\gtrsim$220°C	$PtAs_2$ (possibly some $PtGa_2$)	FeS_2-type (cubic) $a_o \simeq 0.597$ nm	$\langle 011\rangle \| \langle 011\rangle_{GaAs}$ $(1\bar{2}2) \| (100)_{GaAs}$ textured	Pt_3Ga, PtGa, possibly $PtGa_2$	Pt, Ga	between PtGa and $PtAs_2$ layers	∼350°C coarsening of $PtAs_2$ grains	$PtGa/PtAs_2/GaAs$ (∼350°C)

a) See Reference 27

b) See Reference 22

REFERENCES

1. J. Tersoff, J. Vac. Sci. Technol. B3, 1157 (1985).

2. O.F. Sankey, R.E. Allen, S-F. Ren and J.D. Dow, ibid, p. 1162.

3. C.B. Duke and C. Mailhiot, ibid, p. 1170.

4. W.E. Spicer, N. Newman, T. Kendelewicz, W.G. Petro, M.D. Williams, C.E. McCants and I. Lindau, ibid, p. 1178.

5. F. Schaffler and G. Abstreiter, ibid, p. 1184.

6. J.M. Woodall and J.L. Freeouf, ibid, 2, 510 (1984).

7. R. Ludeke, T.-C. Chiang and T. Miller, ibid, 1, 581 (1983).

8. N. Braslau, J. Vac. Sci. Technol. 19, 803 (1981).

9. T.J. Lewis, J. Appl. Phys. 26, 1405 (1955).

10. S. Leung, T. Yoshiie, C.L. Bauer and A.G. Milnes, J. Electrochem. Soc. 132, 898 (1985).

11. W.T. Anderson, Jr., A. Christou and J.E. Davey, J. Appl. Phys. 49, 2998 (1978).

12. E.D. Marshall, W.X. Chen, C.S. Wu, S.S. Lau and T.F. Kuech, Appl. Phys. Lett. 47, 298 (1985).

13. S.R. Smith and J.S. Solomon, Mat. Lett. 3, 294 (1985).

14. K. Tsutsui and S. Furukawa, J. Appl. Phys. 56, 560 (1984).

15. T. Sands, V.G. Keramidas, R. Gronsky and J. Washburn, Thin Solid Films 136, 105 (1986).

16. N. Braslau, J.B. Gunn and J.L. Staple, Solid-State Electron. 10, 381 (1967).

17. G.Y. Robinson, Solid-State Electron. 18, 331 (1975).

18. T.S. Kuan, P.E. Batson, T.N. Jackson, H. Rupprecht and E.L. Wilkie, J. Appl. Phys. 54, 6952 (1983).

19. Z. Liliental-Weber, N. Newman, W.E. Spicer, R. Gronsky, J. Washburn and E.R. Weber, Mat. Res. Soc. Symp. Proc., Thin Films-Interfaces and Phenomena, Fall Meeting, 1985, in press.

20. R.S. Williams, J.R. Lince and T.-C. Tsai, ibid.

21. M. Ogawa, Thin Solid Films 70, 181 (1980).

22. A. Lahav, M. Eizenberg and Y. Komen, Mat. Res. Soc. Symp. Proc. 37, 641 (1985).

23. T. Sands, V.G. Keramidas, J. Washburn and R. Gronsky, Appl. Phys. Lett. 48, 402 (1986).

24. A.K. Sinha, T.E. Smith and M.J. Levinstein, IEEE Trans. Electron Devices ED-22, 218 (1975).

25. J.O. Olowolafe, P.S. Ho, M.J. Hovel, J.E. Lewis and J.M. Woodall, J. Appl. Phys. 50, 955 (1979).

26. X-F. Zeng and D.D.L. Chung, J. Vac. Sci. Technol. 21, 611 (1982).

27. T.S. Kuan, J.L. Freeouf, P.E. Batson and E.L. Wilkie, J. Appl. Phys. 58, 1519 (1985).

28. T. Sands, V.G. Keramidas, R. Gronsky and J. Washburn, Mat. Lett. 3, 409 (1985).

29. T.S. Kuan, Mat. Res. Soc. Symp. Proc. 31, 143 (1984).

30. T. Sands, V.G. Keramidas, A.J. Yu, K.M. Yu, R. Gronsky and J. Washburn, Mat. Res. Soc. Symp. Proc., Thin Films-Interfaces and Phenomena, Fall Meeting, 1985, in press.

31. P. Oelhafen, J.L. Freeouf, T.S. Kuan, T.N. Jackson and P.E. Batson, J. Vac. Sci. Technol. B1, 588 (1983).

32. N. Toyoda, M. Mochizuki, T. Mizoguehi,R. Nii and A. Hojo, GaAs and Related Compounds, 1981, edited by T. Sugano, Inst. Phys. Conf. Ser. No. 63 (Institute of Physics, Bristol, 1982) p. 521.

33. A.K. Sinha and J.M. Poate in Thin Films-Interdiffusion and Reactions edited by J.M. Poate, K.N. Tu and J.W. Mayer (Wiley, New York 1978) p. 417.

34. A.K. Sinha and J.M. Poate, Appl. Phys. Lett. 23, 666 (1973).

35. C. Fontaine, T. Okumura and K.N. Tu, J. Appl. Phys. 54, 1404 (1983).

36. T. Sands, Mat. Res. Soc. Symp. Proc., Materials Problem Solving with the Transmission Electron Microscope, Fall Meeting, 1985, in press.

37. G. Cliff and G.W. Lorimer, J. Micros. 103, 203 (1975).

38. L.R. Doolittle, Nucl. Instrum. Methods B9, 344 (1985).

39. L.J. Chen and Y.F. Hsieh, Proc. 41st, Ann. Meeting. Electron Micros. Society of America, edited by G.W. Bailey (San Francisco Press, S.F., 1983) p. 156.

40. W.B. Pearson, Handbook of Lattice Spacings and Structures of Metals and Alloys (Pergamon, New York, 1958) p. 695 and F. Laves and H.J. Wallbaum, Z. angew. Min. 4, 17 (1941-42).

41. M. Hansen, Constitution of Binary Alloys (McGraw-Hill, N.Y. 1958) p. 750 and E. Hellner and F. Laves, Z. Naturforsch 2a, 177 (1947).

42. S.H. Chen, C.B. Carter, C.J. Palmstrøm and T. Ohashi, Mat. Res. Soc. Symp. Proc., Thin Films - Interfaces and Phenomena, Fall Meeting, 1985, in press.

43. R.D. Heyding and L.D. Calvert, Can J. Chem. 35, 1205 (1957).

44. R. Beyers, R. Sinclair and M.E. Thomas, J. Vac. Sci. Technol. B2, 781 (1984).

45. T. Sands, K.M. Yu, S.K. Cheung and V.G. Keramidas, Proc. 1986 Northeast Regional Meeting on Semiconductor-based Heterostructures: Interfacial Structure and Stability, May 1986, TMS-AIME, in press.

46. K.M. Yu, J. Jaklevic and E.E. Haller, Mat. Res. Soc. Symp. Proc., Materials Characterization, Spring Meeting, 1986, in press.

47. V. Kumar, J. Phys. Chem. Solids 36, 535 (1975).

48. C.C. Chang, S.P. Murarka, V. Kumar and G. Quintana, J. Appl. Phys. 46, 4237 (1975).

49. A.J. Yu, G.J. Galvin, C.J. Palmstrøm and J.W. Mayer, Appl. Phys. Lett. 47, 934 (1985).

50. A.J. Yu and C.J. Palmstrøm, private communication.

FIGURE CAPTIONS

Fig.1 Cross-sectional TEM images of Ni/GaAs, Pd/GaAs and Pt/GaA as-deposited and annealed at 220, 315 and 410°C. Morphology of Pd/GaAs samples annealed at 315 and 410°C is laterally nonuniform (see Fig. 14) and cannot be represented in this Figure. Scale marker in lower right applies to all micrographs. (XBB 857-5850).

Fig.2 Plan-view TEM image of Ni/GaAs sample annealed at 315°C for 10 min. Note hole where unreacted Ni patch has been lifted off by the etchant. Compare with cross-sectional micrograph in Fig. 3. (XBB 858-6329).

Fig.3 Cross-sectional TEM image of Ni/GaAs sample annealed at 220°C for 10 min. Native oxide-hydrocarbon layer has prevented the reaction locally. (XBB 855-4168).

Fig.4 Summary of layer thickness measurements from Fig. 3 and similar images. Image magnifications were calibrated using lattice images of adjacent GaAs substrate. (XBL 8511-4654).

Fig.5 EDS spectra from Ni-Ga-As samples. (a) Spectrum obtained with 15 nm probe from cross-sectional TEM specimen of sample annealed at 220°C for 10 min. (b) Spectrum obtained with 15 nm probe from plan-view TEM specimen of sample

annealed at 315°C for 10 min. Spectra in (c) and (d) were obtained with 20 nm probe from grains near surface and interface, respectively, in cross-sectional TEM specimen of sample annealed at 480°C for 10 min. Copper K_α peak in spectra from cross-sectional specimens results from stray electrons striking Cu support grid. (XBL 862-503).

Fig.6 RBS spectrum and simulation for Ni/GaAs sample annealed at 220°C for 10 min. Simulation is based on input from TEM study (90% Ni_3GaAs, 10% unreacted Ni). (XBL 859-3986).

Fig.7 (a) Diffraction pattern from cross-sectional TEM specimen of Ni_3GaAs/GaAs. Two variants of Ni_3GaAs in $\langle\bar{2}\bar{1}10\rangle$ zone-axis orientation are readily distinguishable. Diffraction pattern from one variant is outlined. Underlined indices indicate GaAs reflections. GaAs is in <011> zone-axis orientation. (b) Diffraction pattern from plan-view specimen of sample annealed at 315°C for 10 min. Diffraction patterns from all four variants overlap. Only pattern from one variant is indexed. Positions of superlattice spots are consistent with a combination of $2a_o \times c_o$ and $3a_o \times c_o$ superstructures. (XBB 862-1254).

Fig.8 Structures of Ni_xX_2 (X = Ga, In or As) phases based on the hexagonal B8 structure. (XBL 859-3952).

Fig.9 Cross-sectional TEM image of Ni/GaAs sample annealed at 480°C for 10 min. White line indicates original depth of the reacted layer after annealing at 220°C for 10 min. Arrowed region is imaged in Fig. 10. (XBB 861-414).

Fig.10 Cross-sectional image of arrowed region in Fig. 9. Approximate composition was determined by EDS (see Fig. 5(d)). $NiAs_{0.6}Ga_{0.4}$ is in $\langle 2\bar{1}\bar{1}0 \rangle$ zone-axis orientation. GaAs is in <011> zone-axis orientation. Note that $\{01\bar{1}2\}_{Ni-As-Ga}$ is approximately parallel to $\{0\bar{1}1\}_{GaAs}$. This orientation relationship is also observed for Ni_3GaAs on GaAs. (XBB 861-413A).

Fig.11 Schematic isothermal sections of the (a) Ni-Ga-As, (b) Pd-Ga-As and (c) Pt-Ga-As thin-film phase diagrams. Ni-Ga-As phase diagram ($T \lesssim 600°C$) includes the observation by Lahav *et al* (Ref. 22) of NiAs and cubic NiGa as the final reaction products. The Pd-Ga-As phase diagram applies to the temperature range 250°C < T < 480°C for ~45 nm Pd deposited on GaAs and annealed in flowing forming gas. The dashed tie lines represent the observation of Pd_2Ga, PdGa and $PdAs_2$ in films annealed

at higher temperatures (500 to 600°C) with SiO_2 caps to prevent excessive sublimation of As.[46] As discussed in the text, the Pd-GaAs reaction is particularly sensitive to film thickness and annealing ambient. The Pt-Ga-As diagram applies to the temperature range T < 500°C. Only compound phases which have been identified as products of M/GaAs thin film reactions are included in these diagrams. (XBL 862-598).

Fig.12 Cross-sectional TEM micrograph of phase I layer formed during deposition of Pd onto (100) GaAs. Note that native oxide-hydrocarbon layer has been broken up by stresses involved in the formation of the atomically rough reacted layer. (XBB 858-6327).

Fig.13 High-resolution cross-sectional TEM image of phase II grain at bottom of deep penetration in sample imaged in Fig. 14 (a)-(c). Note that adjacent grains of phase I have different orientations. Phase I, phase II and GaAs are in [0001], [0001] and $[01\bar{1}]$ zone-axis orientations, respectively. (XBB 850-9418).

Fig.14 Series of cross-sectional TEM images showing development of phase II penetrations. Images (a)-(c) are from

different regions of sample annealed at 275°C for 10 min. after deposition of 45 nm Pd. Image (d) is from sample annealed at 315°C for 10 min. Deep penetrations are 1-2μm apart. (XBB 850-9419).

Fig.15 RBS spectra from Pt/GaAs samples annealed at 220, 315 and 410°C. Deconvolution of spectrum from sample annealed at 410°C is consistent with Pt-Ga/$PtAs_2$/GaAs layer sequence. Pt-Ga is primarily PtGa as determined by electron diffraction. Small amounts of Pt_3Ga and $PtGa_2$ may also be present. (XBL 862-543).

Fig.16 High-resolution TEM image of $PtAs_2$/GaAs interface after annealing at 410°C for 10 min. Note the twin relationship between $PtAs_2$ and GaAs. Both phases are in <011> zone-axis orientation. (XBB 858-6328).

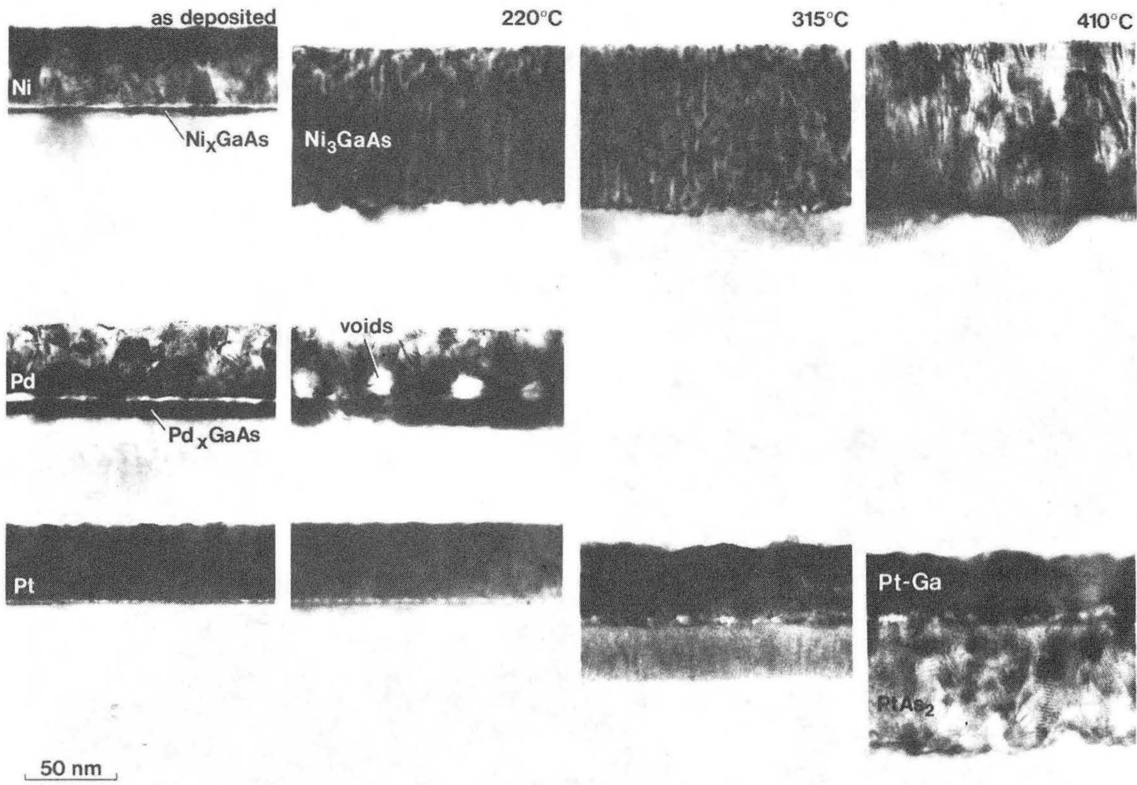

XBB 857-5850

Fig. 1

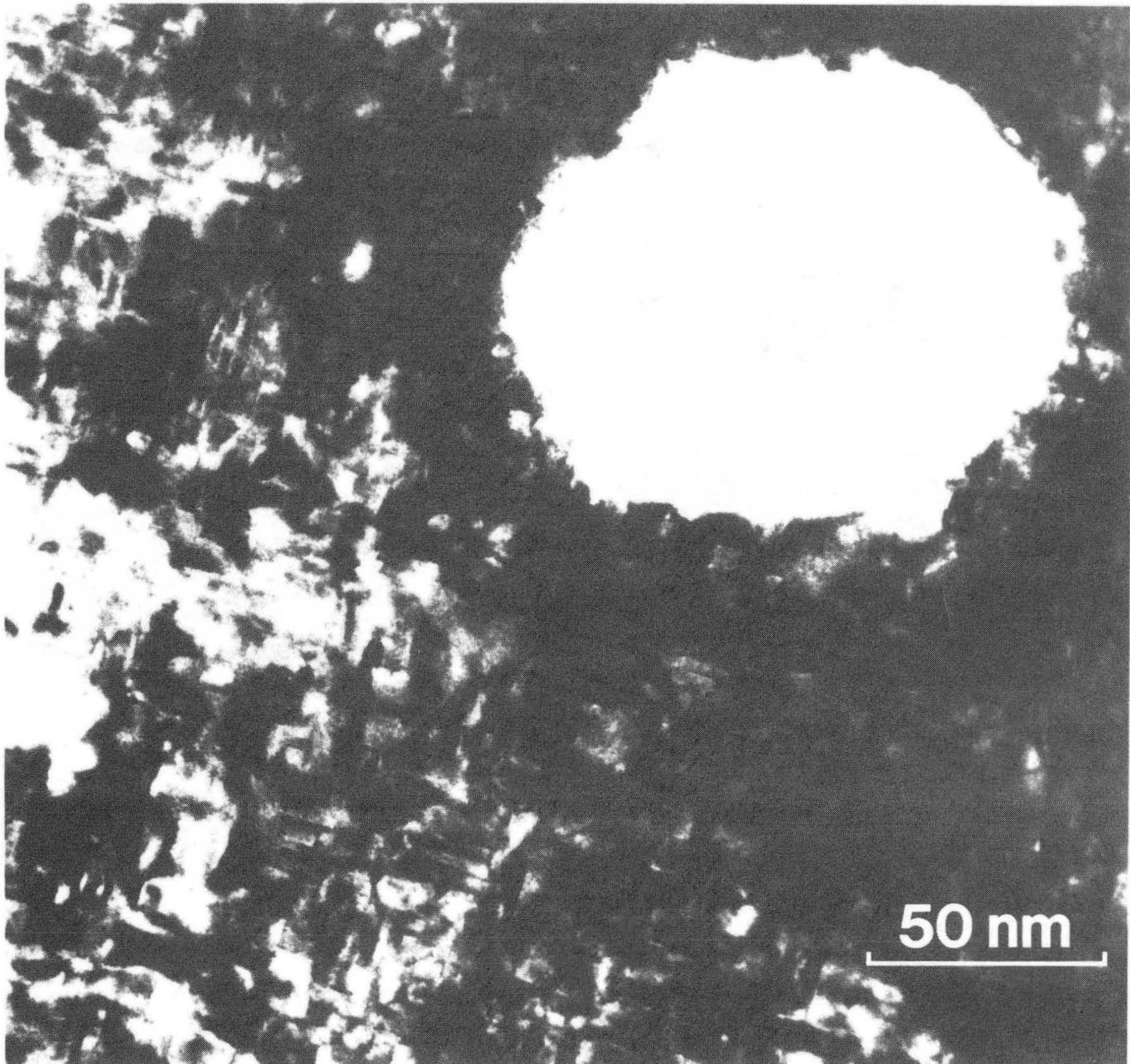

XBB 858-6329

Fig. 2

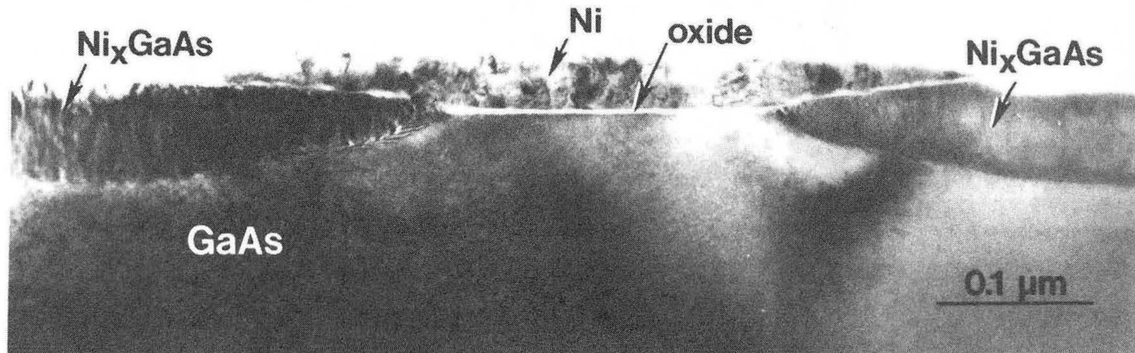

XBB 855-4168

Fig. 3

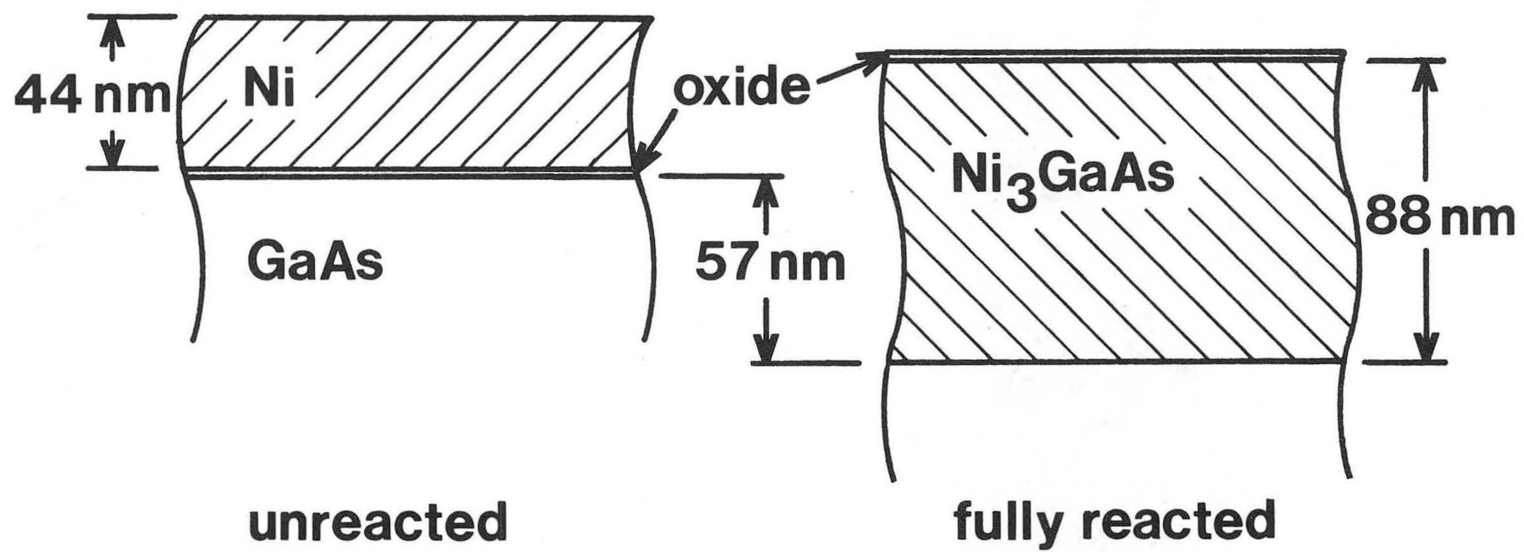

XBL 8511-4654

Fig. 4

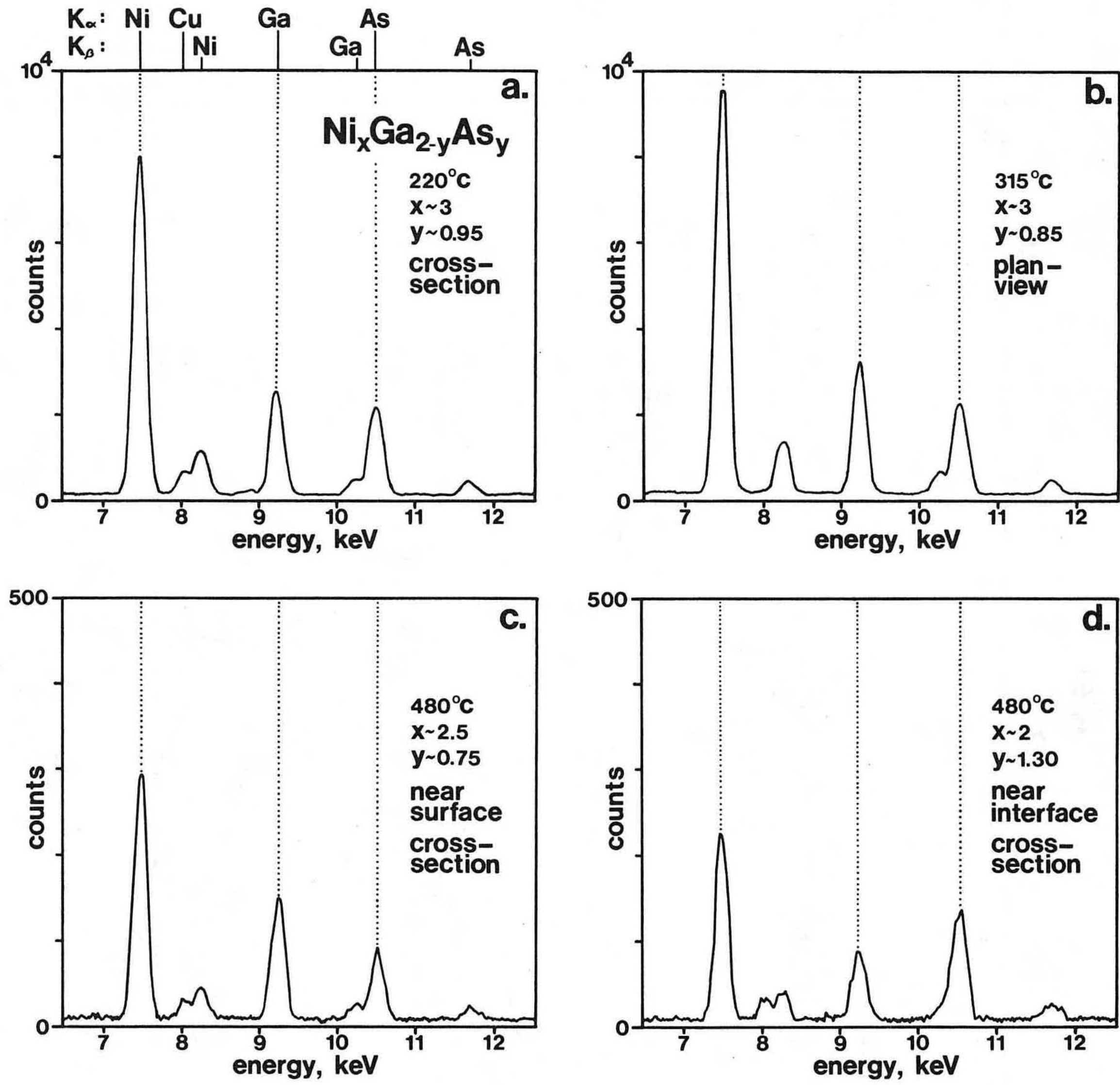

XBL 862-503

Fig. 5

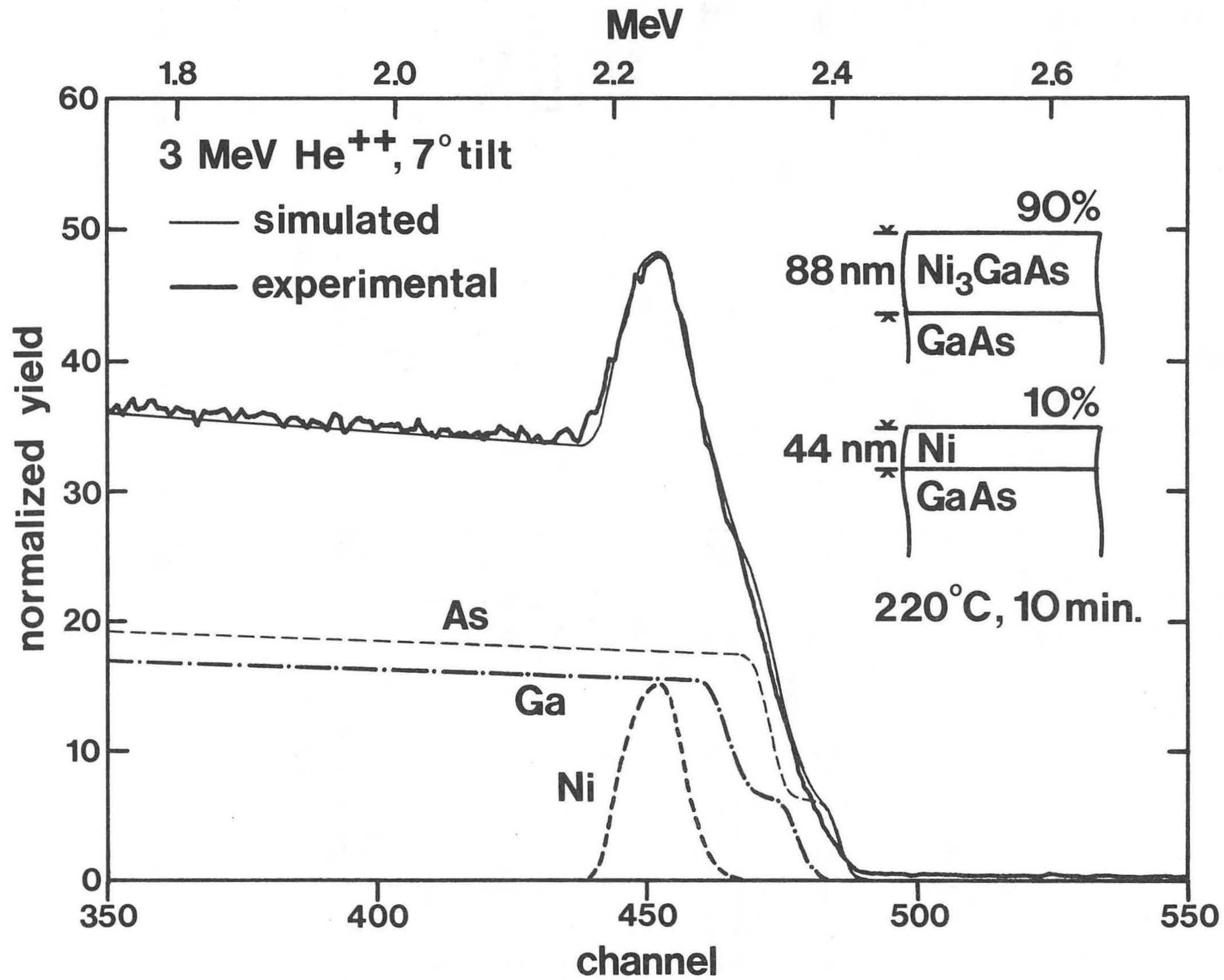

XBL 859-3986

Fig. 6

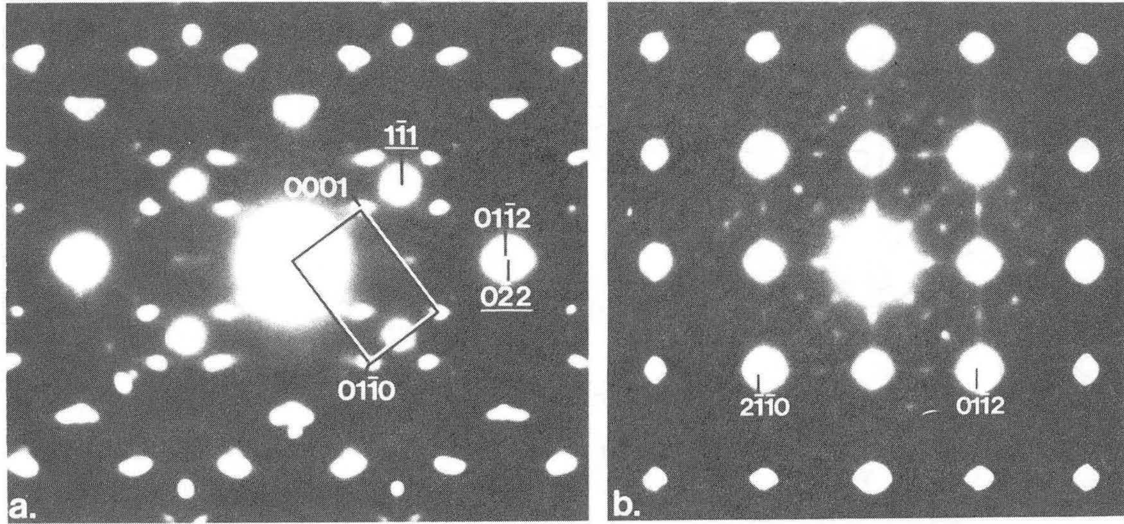

XBB 862-1254

Fig. 7

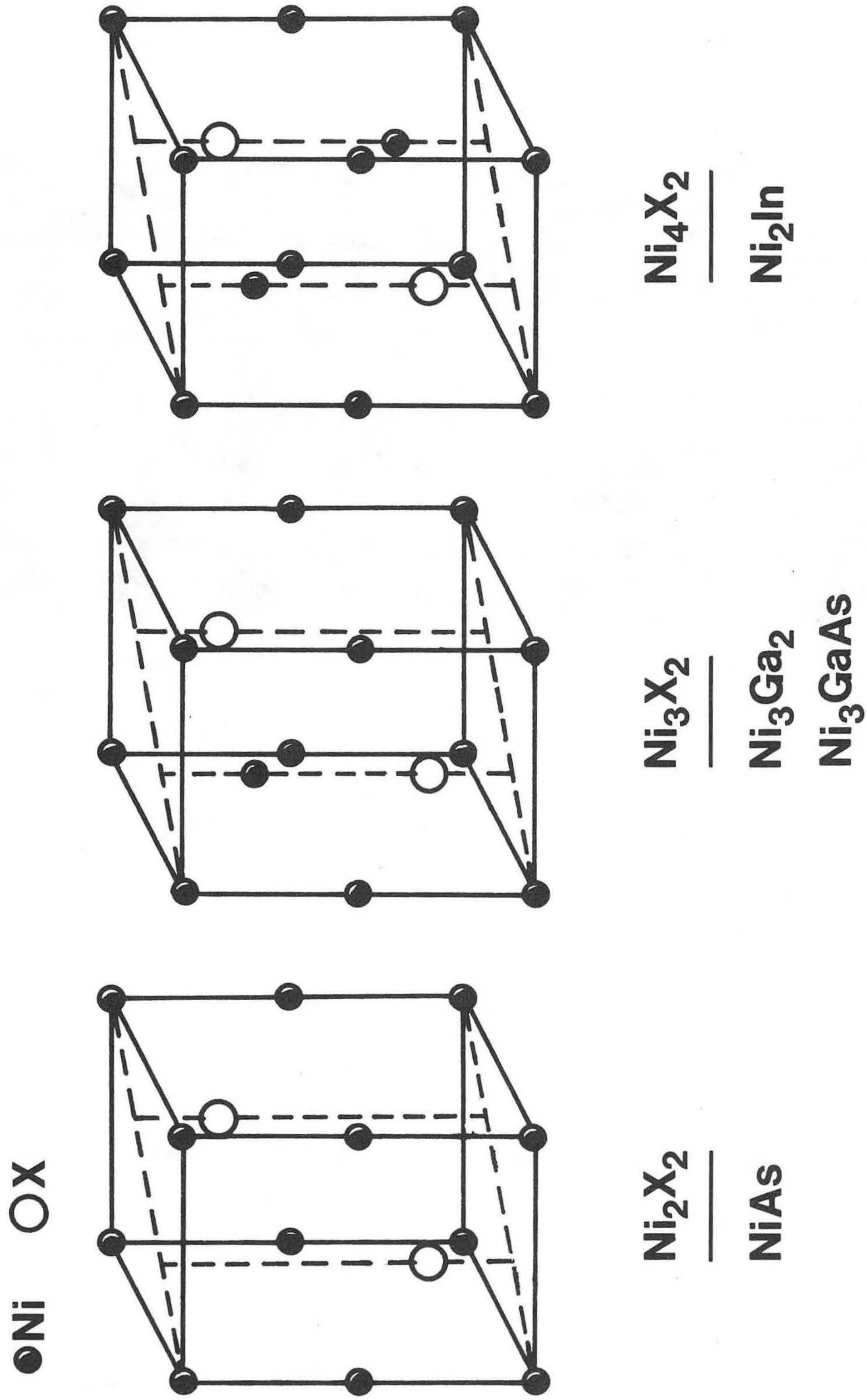

XBL 859-3952

Fig. 8

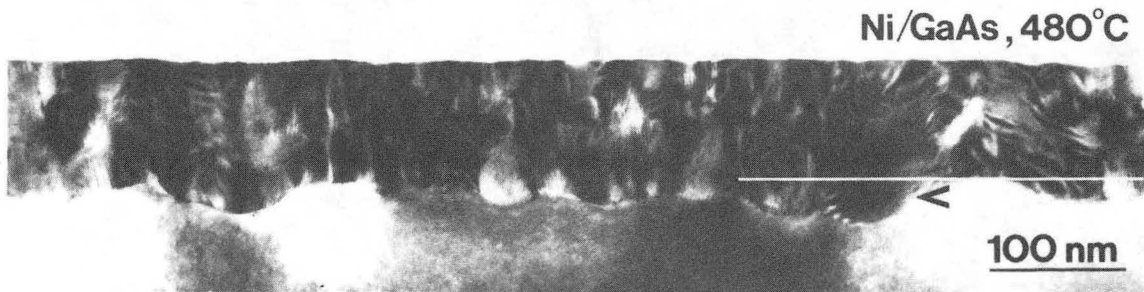

XBB 861-414

Fig. 9

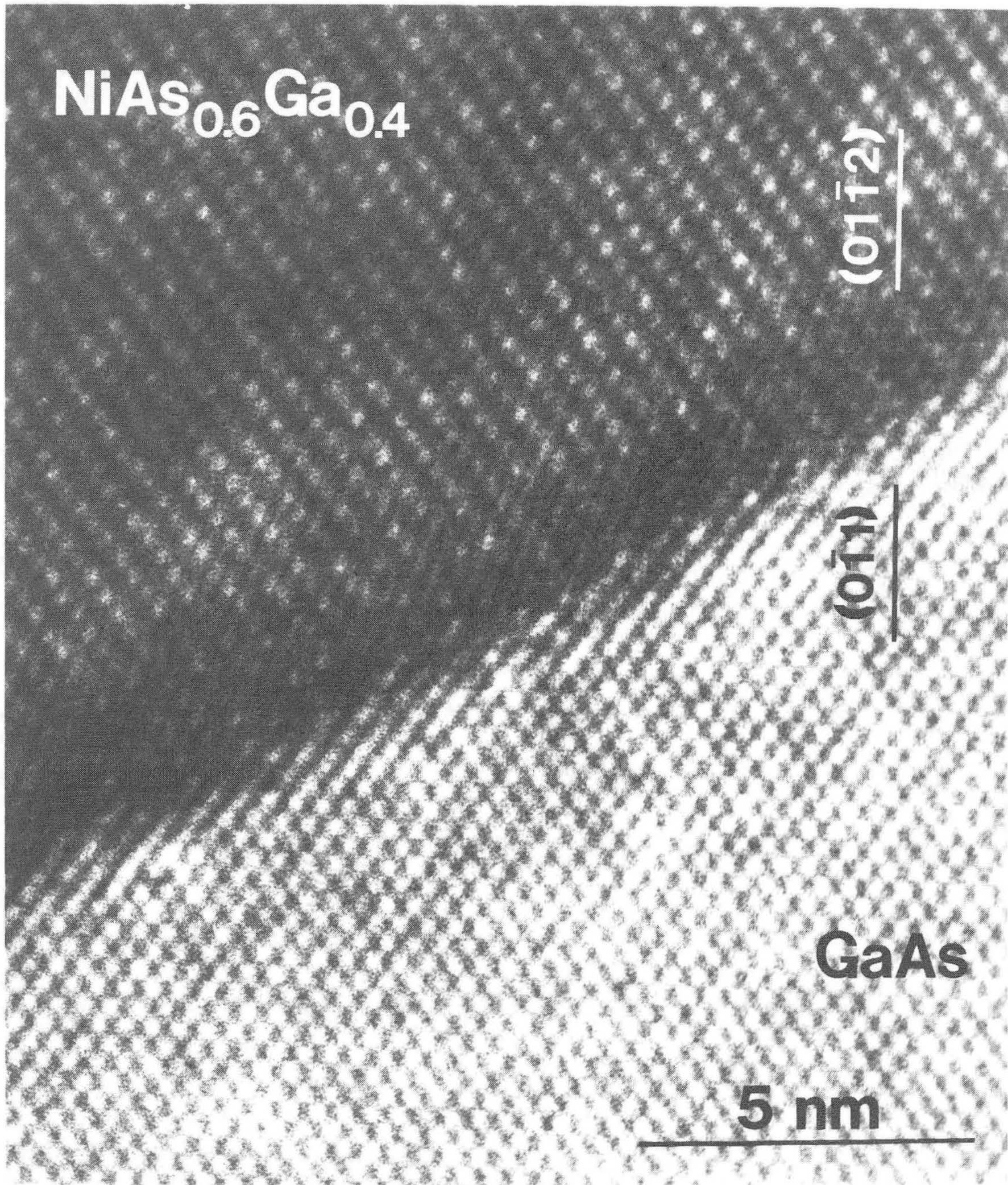

XBB 861-413-A

Fig. 10

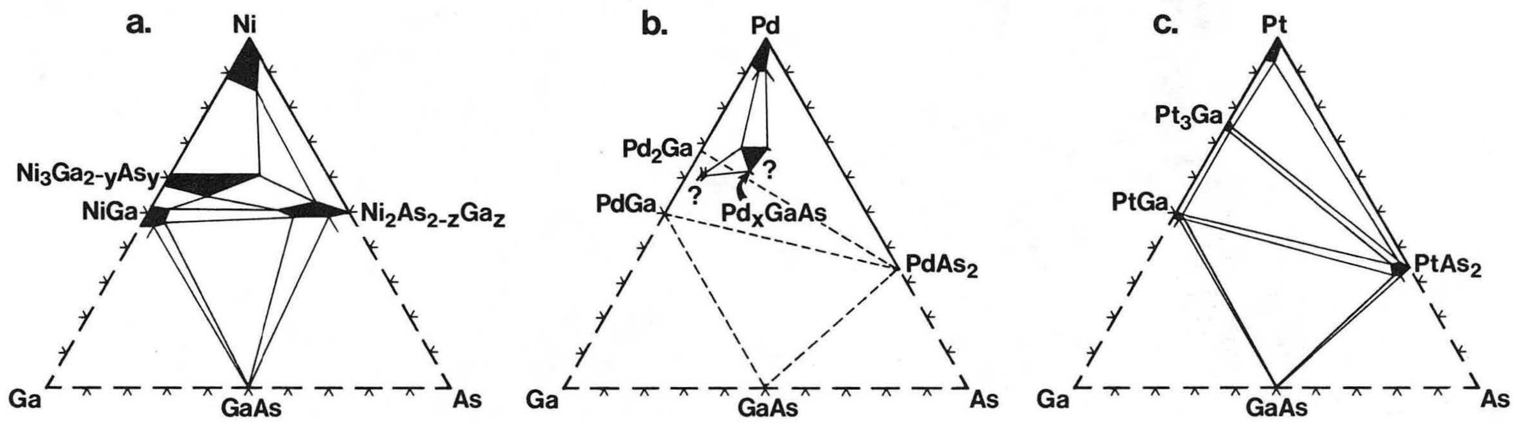

Fig. 11

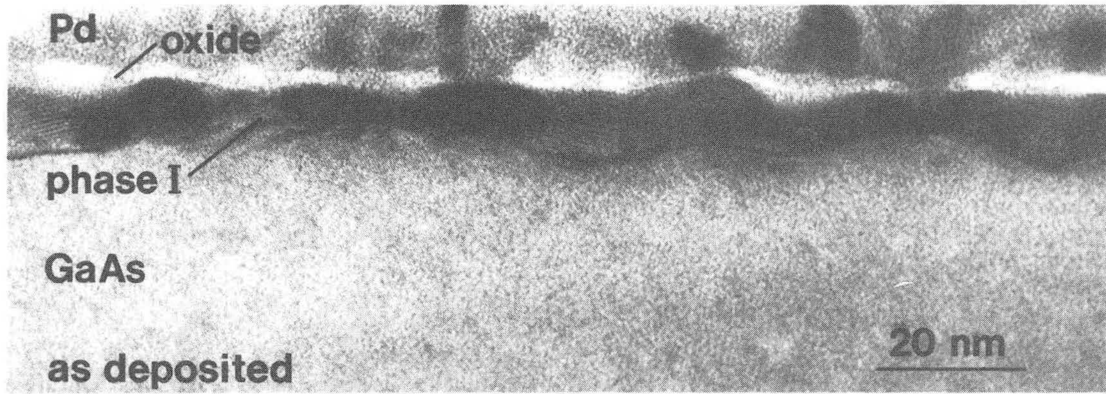

XBB 858-6327

Fig. 12

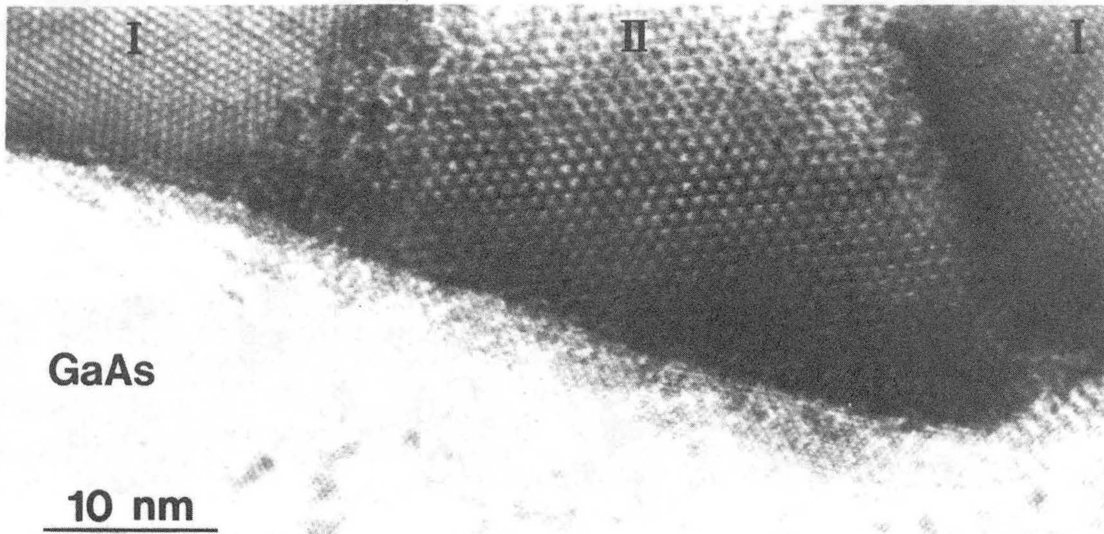

XBB 850-9418

Fig. 13

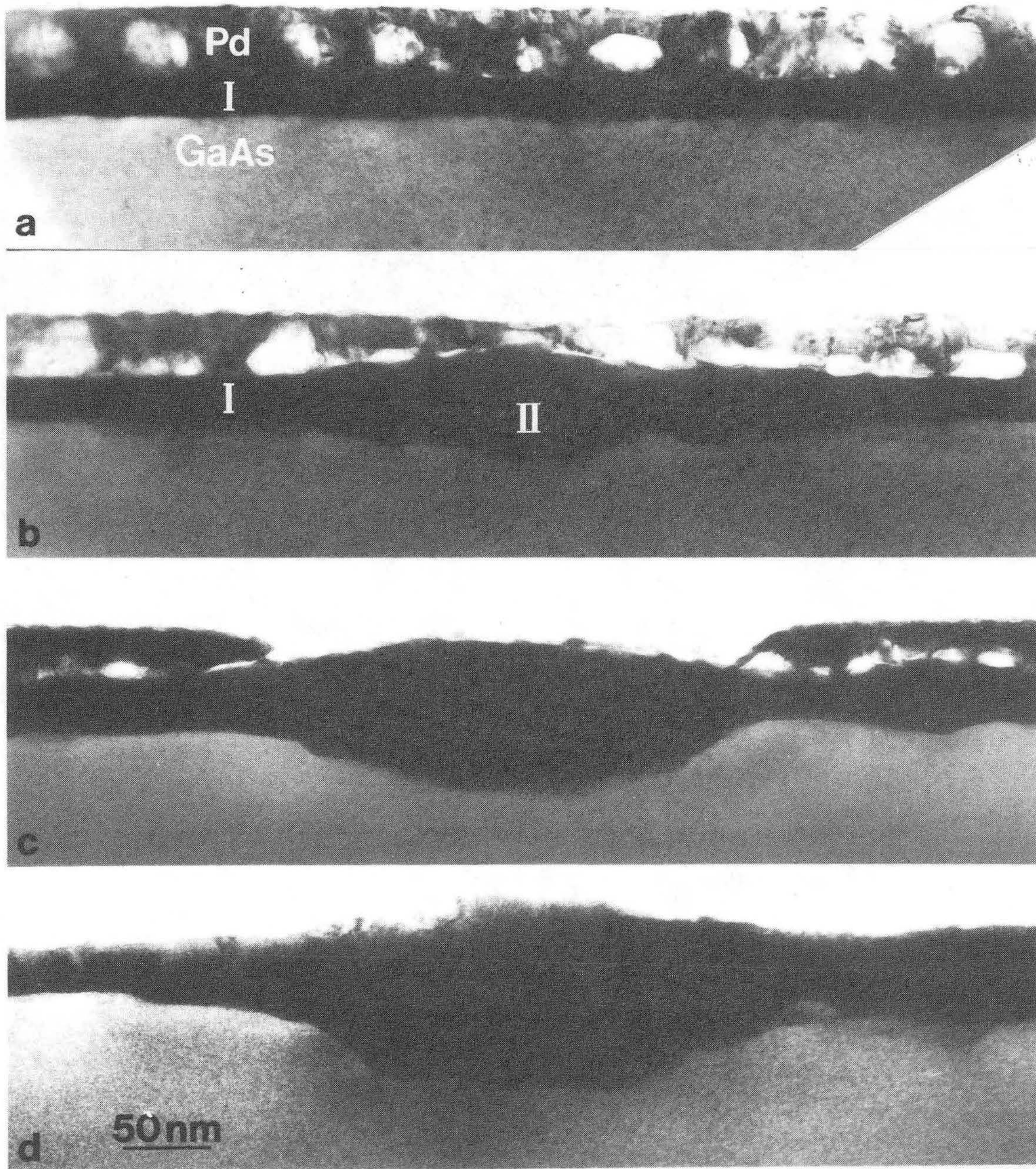

XBB 850-9419

Fig. 14

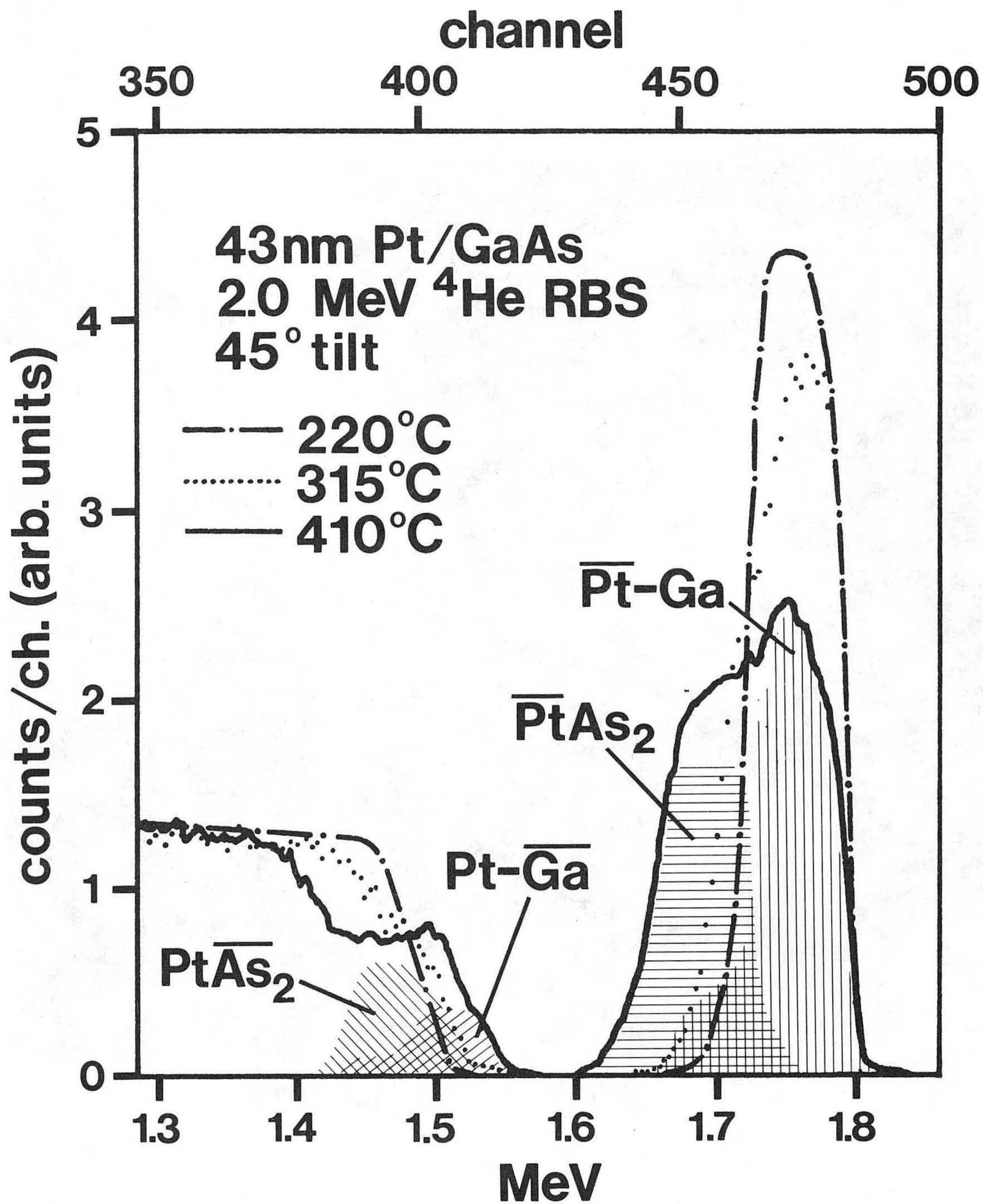

XBL 862-543

Fig. 15

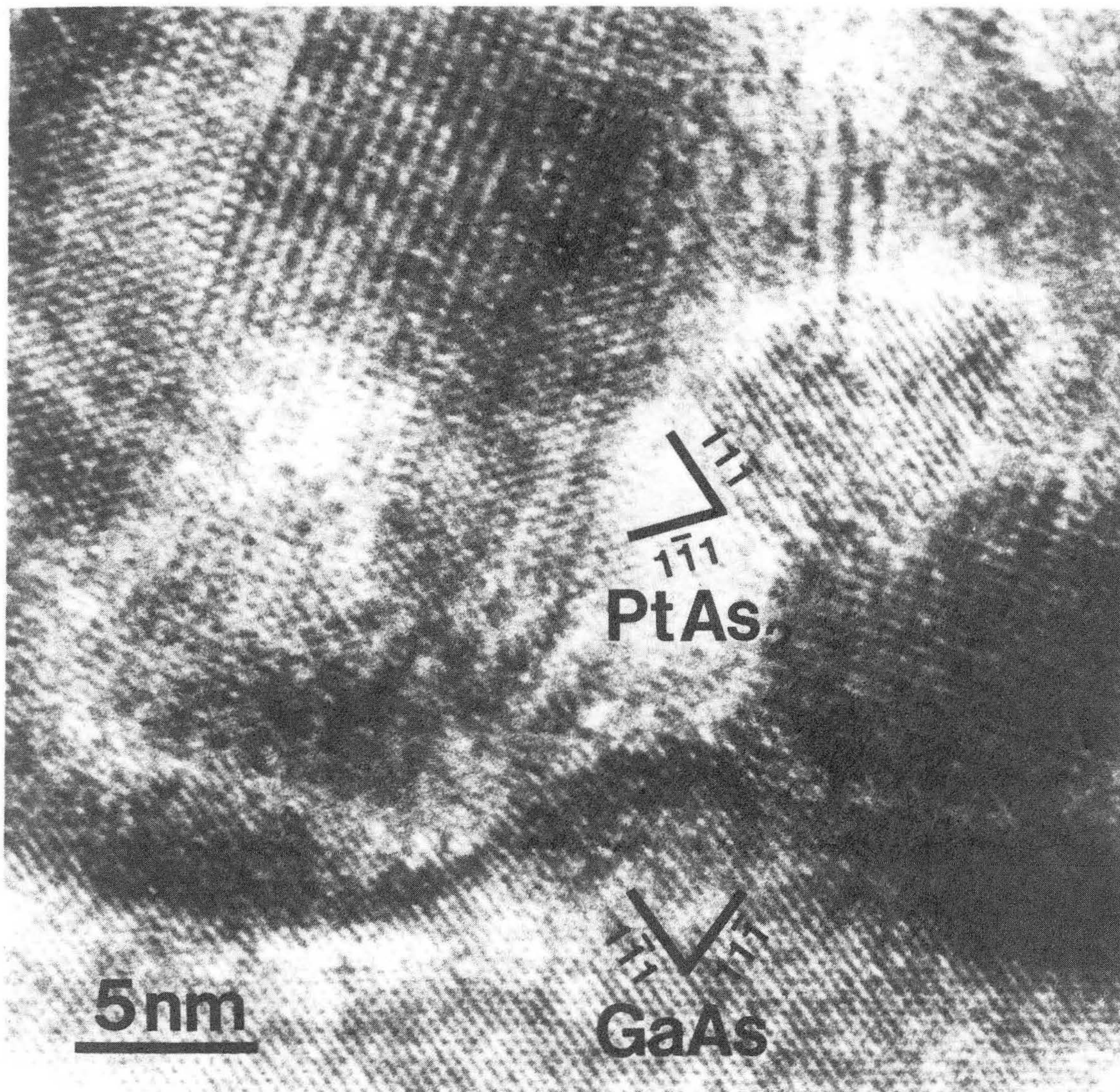

XBB 858-6328

Fig. 16

This report was done with support from the Department of Energy. Any conclusions or opinions expressed in this report represent solely those of the author(s) and not necessarily those of The Regents of the University of California, the Lawrence Berkeley Laboratory or the Department of Energy.

Reference to a company or product name does not imply approval or recommendation of the product by the University of California or the U.S. Department of Energy to the exclusion of others that may be suitable.

LAWRENCE BERKELEY LABORATORY
TECHNICAL INFORMATION DEPARTMENT
UNIVERSITY OF CALIFORNIA
BERKELEY, CALIFORNIA 94720